

Cucurbituril-Based Porphyrin Cascade Assembly for Cell Imaging and Targeted Drug Delivery

Xing Yuan, De-Fang Xu, Yahui Song, Ying-Ming Zhang,* and Yu Liu*

Cite This: *ACS Appl. Polym. Mater.* 2024, 6, 4331–4338

Read Online

ACCESS |

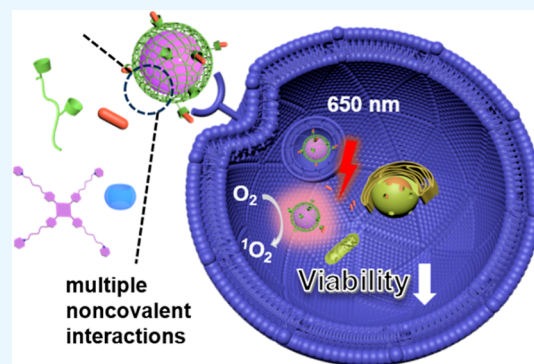
Metrics & More

Article Recommendations

Supporting Information

ABSTRACT: Supramolecular assemblies based on multiple host–guest interactions have aroused widespread interest in the fabrication of innovative biomaterials. In this work, a combinational nanosupramolecule is constructed by an orthogonal two-step self-assembling process. The generation efficiency of reactive oxygen species and fluorescence emission intensity of pyridinium-appended porphyrin are greatly enhanced upon inclusion complexation with cucurbit[8]uril. Meanwhile, the introduction of β -cyclodextrin-grafted hyaluronic acid can facilitate the formation of secondary assemblies and endow them with the desired targeting ability toward cancer cells. After carrying doxorubicin hydrochloride as the loaded cargo, the resultant supramolecular nanoparticles exhibit much higher anticancer activity at the cellular level upon the near-infrared light irradiation. To be envisioned, such nanosupramolecular assemblies featuring both advantageous photodynamic and chemotherapeutic effects may be developed as more promising nanoplatforms for disease diagnosis and treatment.

KEYWORDS: host–guest chemistry, molecular assembly, photodynamic effect, fluorescent cell imaging, targeted drug delivery



INTRODUCTION

The host–guest complexation based on cavity-bearing macrocycles have recently stimulated an upsurge of interest in biomedical science and materials, mainly due to the dynamic reversibility of noncovalent interactions.^{1–6} This feature can allow us to design and fabricate more advanced supramolecular nanoassemblies for disease diagnostics and therapeutics.^{7–12} In this regard, two representative macrocycles, cyclodextrins (CDs) and cucurbiturils (CBs), have been drawn into the limelight because of their immense advantages in molecular recognition and assembly. Concretely, the former as a family of glucose-derived cyclic oligomers can be functionalized to accommodate diverse guests mainly through hydrophobic interactions.^{13,14} The CD-involved active pharmaceutical ingredients can dramatically enhance water solubility, environmental adaptability, delivery efficiency of parent drugs, thus making many success stories from fundamental research to practical application.^{15–17} The latter as a family of glycoluril-derived cyclic oligomers can selectively encapsulate positively charged guests via hydrophobic and ion–dipole interactions.^{18–20} Therefore, given their complementary molecular binding properties, the combined use of CDs and CBs in a single supramolecular entity represents an increasingly significant and feasible strategy in attaining biocompatible nanoassemblies with elaborate biofunctions.^{21,22}

More remarkably, CDs and CBs can offer a confined and rigidified microenvironment to freeze the molecular conformation of optically active substrates and suppress the

nonradiative relaxation process, thus leading to the emergence of light-activated supramolecular theranostic nanosystems with exceptional photophysical performance.²³ For example, Liu and co-workers recently reported a 6-bromoisoquinoline-involved multicomponent supramolecular assembly as donors by a two-step assembling method, followed by doping a small amount of sulfonated porphyrin as acceptors.²⁴ The coexistence of β -CD and CB[7] could synergistically induce strong room-temperature phosphorescence energy transfer for targeted near-infrared imaging of living tumor cells. Xu et al. reported a positively charged porphyrin, which showed adaptable antibacterial performance upon complexation with CB[7] in the anaerobic and aerobic environment by photothermal and photodynamic pathways, respectively.²⁵ Mao and Kitagishi also constructed a host–guest inclusion complex between a PEGylated tetraphenylporphyrin and a per-O-methylated CD dimer by the molecular threading process. This kind of host–guest complex with O₂-binding characteristics can act as an artificial O₂ carrier in vivo.²⁶ These fascinating results jointly demonstrate that macrocycle-based

Received: February 23, 2024

Revised: March 18, 2024

Accepted: March 20, 2024

Published: March 29, 2024



Scheme 1. Schematic Illustration of TPP-PY@CB[8]@HACD Assembly Loaded with DOX

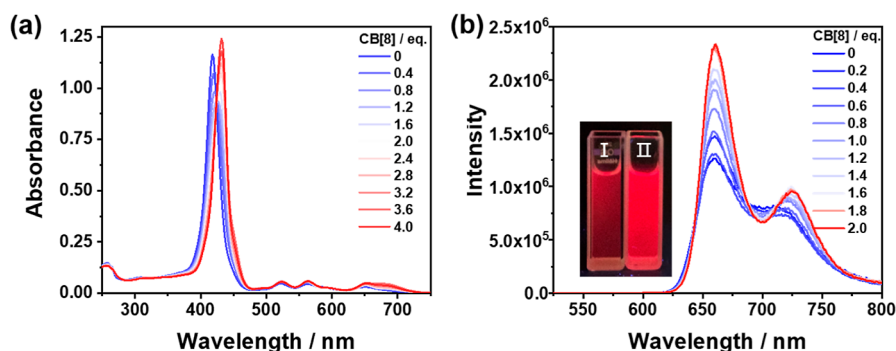
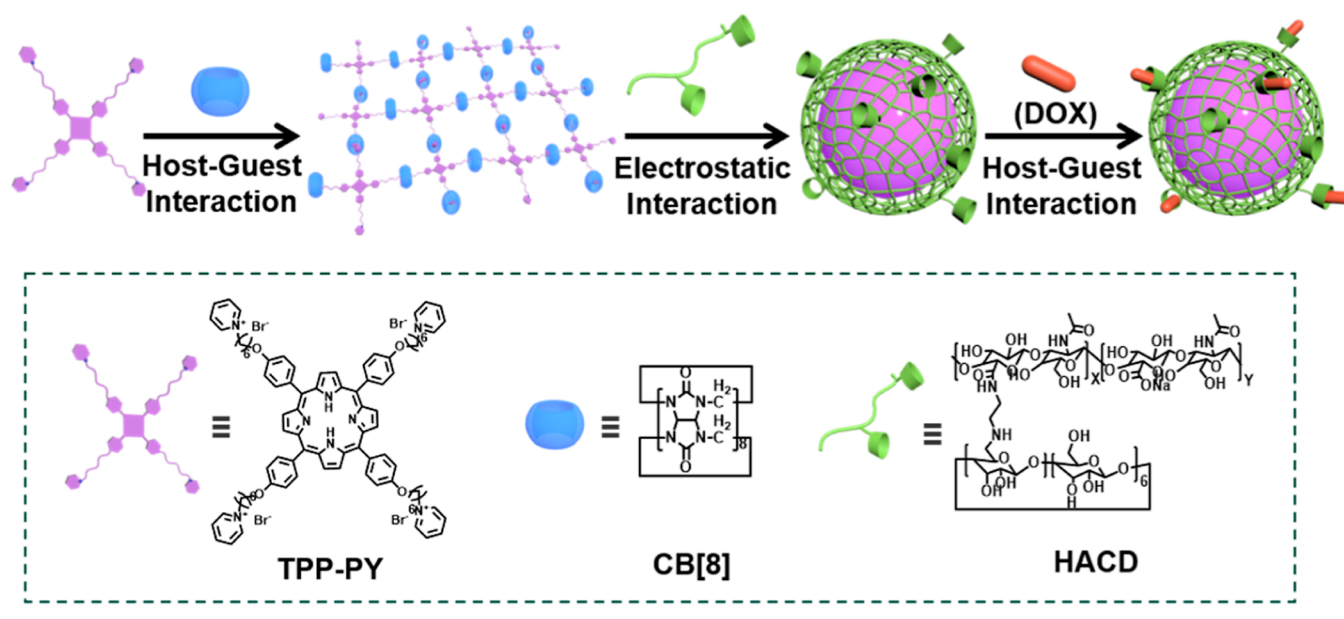


Figure 1. (a) UV-vis absorption and (b) fluorescence spectra of TPP-PY upon addition of CB[8] in aqueous solution at 25 °C ([TPP-PY] = 5 μ M and [CB[8]] = 0–20 μ M). Inset: photographic images of the aqueous solutions of (I) free TPP-PY and (II) TPP-PY@CB[8] complex upon illumination with UV light under ambient conditions.

nanoassemblies hold great potential in attaining functional materials.

Inspired by our ongoing interest in constructing biorelated photoluminescent nanoassemblies, we herein report a supramolecular codelivery system for photosensitizers and drug molecules based on the multiple host–guest interactions with CB[8] and β -CD-grafted hyaluronic acid (HACD, Scheme 1). First, the complexation with CB[8] can dramatically promote the fluorescence emission intensity of pyridinium-appended porphyrin (TPP-PY) by suppressing its intermolecular π – π stacking interaction. Next, HACD, a polysaccharide drug carrier capable of selectively recognizing cancer cells, was further introduced to facilitate the formation of particulate assemblies via multiple electrostatic attraction. Consequently, the obtained TPP-PY@CB[8]@HACD assembly loaded with doxorubicin hydrochloride (DOX) gave more potent killing ability and phototoxicity against cancer cells. Overall, it is anticipated that this work can provide more insights for developing innovative supramolecular theranostic agents.

RESULTS AND DISCUSSION

Synthesis and Host–Guest Complexation. The tetracationic TPP-PY was synthesized by the reaction of tetrahalide

and pyridine in a moderate yield and fully characterized by ^1H NMR and mass spectroscopy (Figures S1–S4, Supporting Information). HACD was synthesized according to the previous literature,²⁷ and the degree of substitution of β -cyclodextrin (β -CD) was determined to be 20.3% by calculating the integral area in ^1H NMR spectrum (Figure S5, Supporting Information).

The molecular binding behaviors of TPP-PY with CB[8] was investigated using UV-vis spectroscopy. Job plot showed a peak at a molar fraction of 0.33, corresponding to the binding stoichiometry of 1:2 (Figure S6a, Supporting Information). Given that one CB[8] molecule is prone to encapsulation with two pyridinium moieties in its cavity, the sheet-like TPP-PY@CB[8] assembly is proposed with extended 1:2 binding stoichiometry (Scheme 1).^{28,29} Accordingly, the binding constants (K) were determined to be $K_1 = 1.52 \times 10^6 \text{ M}^{-1}$ and $K_2 = 7.32 \times 10^5 \text{ M}^{-1}$ using a nonlinear least-squares curve-fitting method (Figure S6b, Supporting Information). The almost same binding strengths in our case further confirmed that the two-step binding process in the TPP-PY@CB[8] complex could not interfere with each other.

The spectroscopic properties were investigated in an aqueous solution. As shown in Figure 1a, one strong absorption peak at 417 nm and three weak ones at 522, 564,

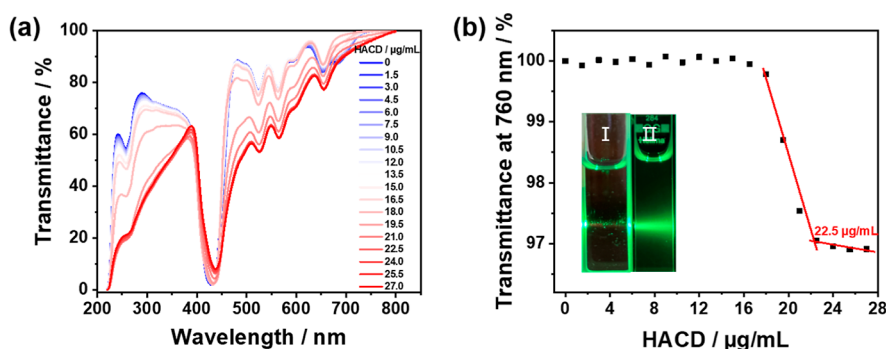


Figure 2. (a) Optical transmittance of TPP-PY \subset CB[8] complex at different concentrations of HACD. (b) Optical transmittance changes of TPP-PY \subset CB[8] complex with the different concentrations of HACD (0–27 $\mu\text{g/mL}$). Inset: Tyndall effect of (I) TPP-PY and (II) TPP-PY \subset CB[8]@HACD assembly ([TPP-PY] = 10 μM and [CB[8]] = 20 μM).

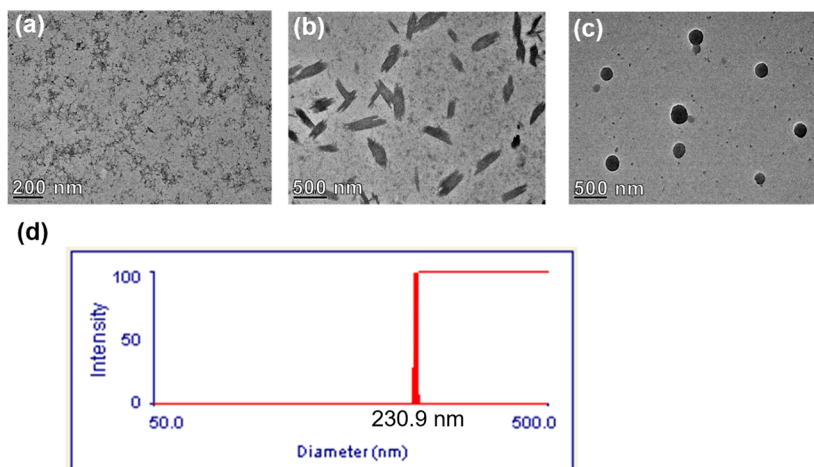


Figure 3. TEM images of (a) TPP-PY, (b) TPP-PY \subset CB[8] complex, and (c) TPP-PY \subset CB[8]@HACD assembly; (d) DLS result of TPP-PY \subset CB[8]@HACD assembly ([TPP-PY] = 10 μM , [CB[8]] = 20 μM , and [HACD] = 22.5 $\mu\text{g/mL}$).

and 648 nm could be observed and assigned to the Soret and Q bands for free TPP-PY, respectively. Upon the gradual addition of CB[8], the absorbance intensity of the Soret band decreased, and a new peak appeared at 432 nm, accompanied by an isosbestic point at 424 nm. In addition, the absorption peaks of the Q-band underwent a clear complexation-induced bathochromic shift, and a new absorption peak appeared at 686 nm. Meanwhile, the fluorescence emission intensity of TPP-PY was gradually enhanced after the continuous addition of CB[8] (Figure 1b). There was two-fold fluorescence enhancement in the presence of CB[8], and it remained basically unchanged in the presence of 2 equiv of CB[8]. Obviously, the molecular confinement by CB[8] can greatly inhibit the intermolecular π - π stacking, and the subsequent aggregation-caused quenching process of TPP-PY, thus leading to the improvement of its photoluminescence performance.³⁰

HACD is well-known to actively target the cell membrane surface receptor CD44 and possess good water solubility, biocompatibility, and biodegradability.³¹ In our case, given the intrinsic carboxylate groups in HA and the pyridinium groups in TPP-PY, the targeted polysaccharide supramolecular assembly may be further fabricated by HACD and the TPP-PY \subset CB[8] complex via electrostatic attraction. With that in mind, the secondary assembly process of TPP-PY \subset CB[8] complex with HACD was investigated by monitoring the changes in optical transmittance. As depicted in Figures 2 and S7 (Supporting Information), the optical transmittance at 760

nm of free TPP-PY remained constant as its concentration increased. In contrast, when HACD was added to the solution of the TPP-PY \subset CB[8] complex, the optical transmittance initially remained constant and then decreased, accompanied by an inflection point at 22.5 $\mu\text{g/mL}$, referring to the formation of ternary nanoaggregates in solution. At this stage, a significant Tyndall effect could also be observed in the TPP-PY \subset CB[8]@HACD solution, once again substantiating the existence of supramolecular nanoassemblies at the optimal molecular composition (Figure 2b, inset). Moreover, it is found that HACD could increase the fluorescence emission intensity of the TPP moiety, and the binary TPP-PY \subset CB[8] complex maintained its fluorescence emission properties in the presence of HACD (Figure S8, Supporting Information).

Along with these observations in the solution phase, the intuitive morphology of TPP-PY, TPP-PY \subset CB[8] complex, and TPP-PY \subset CB[8]@HACD assembly was characterized by transmission electron microscopy (TEM). As shown in Figure 3a–c, free TPP-PY was in an amorphous form, whereas the TPP-PY \subset CB[8] complexation gave uniform nanosheets with about 500 nm in length by the extended intermolecular 1:2 binding stoichiometry. Remarkably, the supramolecular TPP-PY \subset CB[8]@HACD assembly gave distinct spherical nanoparticles of about 200 nm in diameter. Accordingly, dynamic light scattering (DLS) analysis demonstrates that the diameter of obtained nanoparticles was 230.9 nm, which is fully consistent with the results obtained from TEM experiments

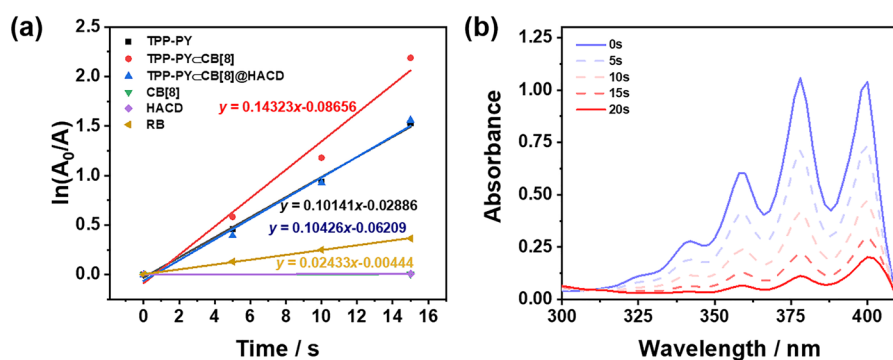


Figure 4. (a) Decomposition rates of ABDA at 378 nm versus irradiation time. (b) UV-vis spectra of ABDA in the presence of TPP-PY \subset CB[8]@HACD assembly under white light irradiation ($\lambda > 420$ nm, [TPP-PY] = 10 μ M, [CB[8]] = 20 μ M, [HACD] = 22.5 μ g/mL, and [ABDA] = 80 μ M).

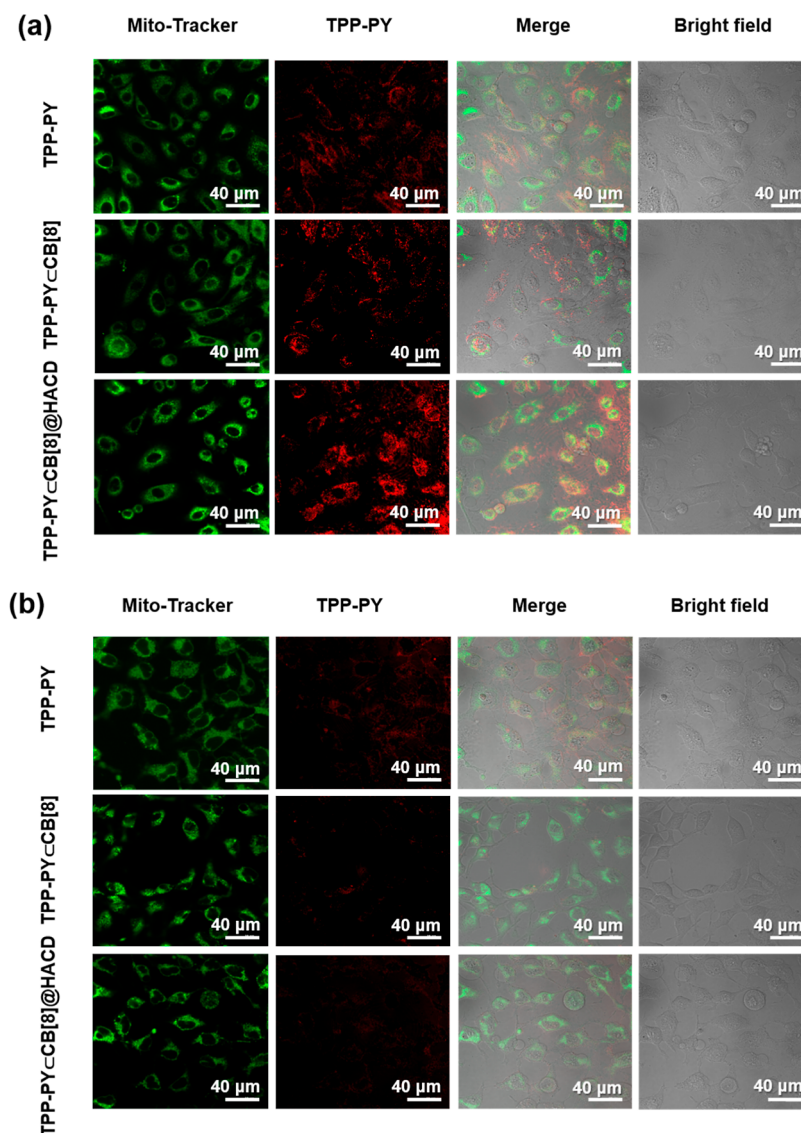


Figure 5. CLSM images in living (a) A549 cells and (b) 293T cells treated with TPP-PY, TPP-PY \subset CB[8] complex, and TPP-PY \subset CB[8]@HACD assembly, respectively. [TPP-PY] = 0.5 μ M, [CB[8]] = 1 μ M, and [HACD] = 1.125 μ g/mL. Mitochondria were stained with Mito-tracker Green. The scale bar is 40 μ m.

(Figure 3d). In addition, no morphological change was observed, suggesting that the obtained ternary assembly could remain stable for at least 48 h (Figure S10a, Supporting

Information). In addition, the TPP-PY \subset CB[8] complex exhibited a zeta potential of 7.21 mV because of the positive charges (Figure S11a, Supporting Information), while this

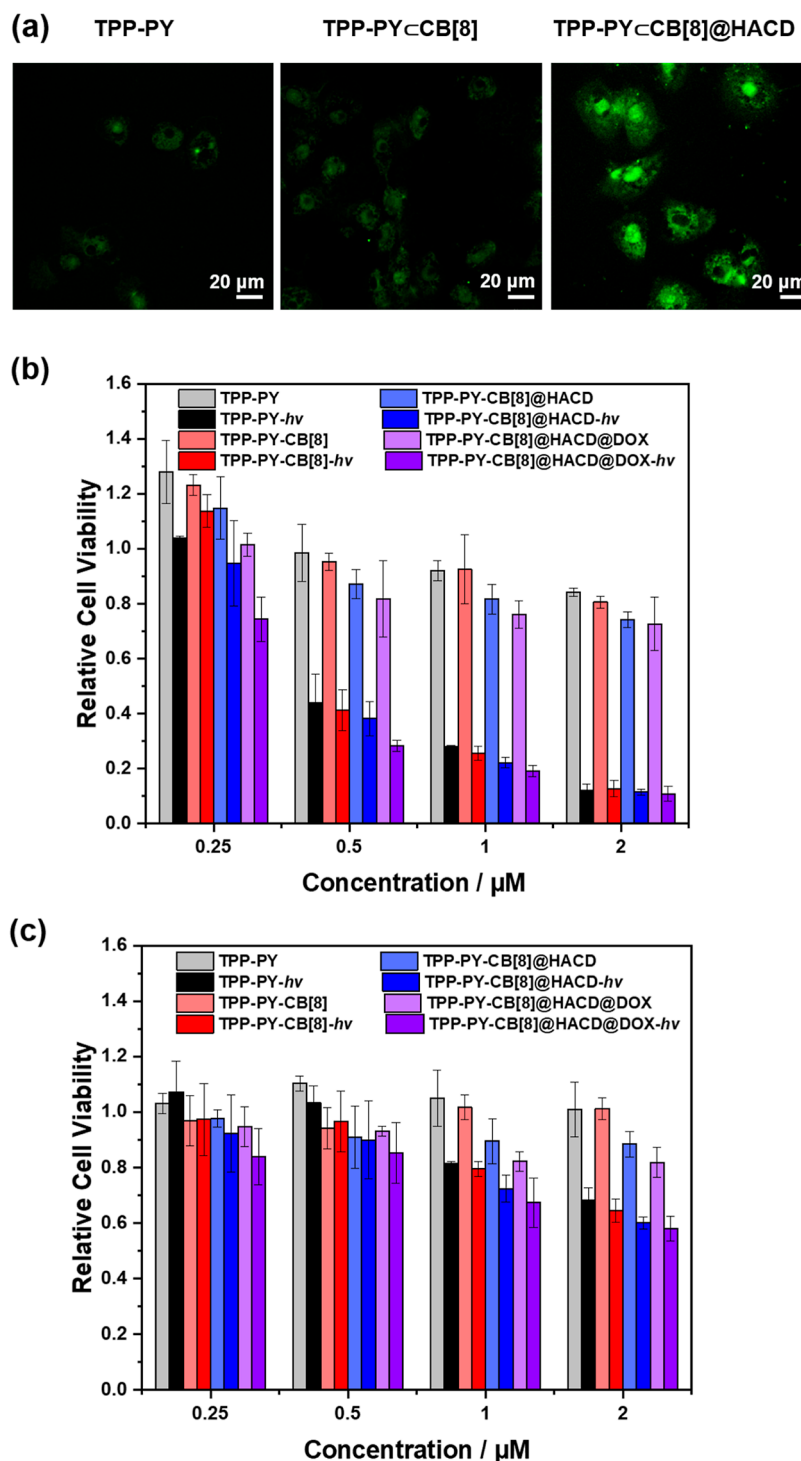


Figure 6. (a) Intracellular $^1\text{O}_2$ detection and distribution in A549 cells treated with TPP-PY, TPP-PY_{CB}[8] complex, and TPP-PY_{CB}[8]@HACD assembly, respectively ($[\text{TPP-PY}] = 0.5 \mu\text{M}$, $[\text{CB}[8]] = 1 \mu\text{M}$, and $[\text{HACD}] = 1.125 \mu\text{g/mL}$). The scale bar is $20 \mu\text{m}$. Cell viability of (b) A549 and (c) 293T cells after incubation with TPP-PY, TPP-PY_{CB}[8] complex, TPP-PY_{CB}[8]@HACD assembly, and TPP-PY_{CB}[8]@HACD@DOX assembly for 12 h with and without light irradiation at 650 nm for 5 min at different concentrations. The concentrations were calculated based on TPP-PY.

value of the TPP-PY_{CB}[8]@HACD assembly was converted to -2.80 mV upon further assembly with HACD (Figure S11b, Supporting Information). These potential changes jointly indicate the close packing of positively charged TPP-PY_{CB}[8] cores with the negatively charged HACD chains through multiple electrostatic interactions, as presented in Scheme 1.

Moreover, the effect of the component-adding sequence on the formation of nanoparticles was further examined. As shown in Figure S10c (Supporting Information), when HACD was added first, the obtained morphology of the TPP-PY/HACD/CB[8] mixture was quite different from the one of TPP-PY_{CB}[8]@HACD assembly. This result demonstrates that encapsulation by CB[8] can greatly inhibit the direct but

undesired interaction between TPP-PY and HACD, which is beneficial for the formation of ternary nanoparticles. In addition, to validate the orthogonal assembling process, the molecular binding behaviors between TPP-PY and HACD were studied using native β -CD as a reference, indicating that the binding affinity is too weak to obtain the reliable K value (Figure S6c, Supporting Information). Therefore, stable TPP-PY/CB[8] complexation can ensure cascade assembly with HACD and consequent drug loading with DOX.

Singlet Oxygen Generation and Drug Loading. 9,10-Anthracenediyl-bis(methylene)dimalonic acid (ABDA) was used as the reactive oxygen species (ROS) indicator to investigate the efficiency of ROS generation by TPP-PY and its supramolecular nanoaggregates, using Rose Bengal (RB) as standard control.^{32–34} As depicted in Figure 4 and Figure S12 (Supporting Information), the UV–vis absorption spectra showed a decrease in absorbance at 378 nm, corresponding to the ROS-induced degradation of ABDA after illumination. The calculation on the singlet oxygen ($^1\text{O}_2$) generation efficiency of free TPP-PY was 2.2 times as high as that of RB (163% versus 75%, Table S1, Supporting Information). In addition, the $^1\text{O}_2$ yields of the TPP-PY/CB[8] complex and TPP-PY/CB[8]@HACD assembly were calculated as 169 and 142%, respectively. It is also noted that the $^1\text{O}_2$ yield of the TPP-PY/CB[8] complex slightly decreased upon addition of HACD. This result is mainly contributed to the morphological changes from loose nanosheets to compact nanoparticles, which may enhance the intermolecular interaction of TPP-PY and then reduce the ROS generation efficiency. Nevertheless, these satisfactory $^1\text{O}_2$ yields can ensure a photodynamic outcome in the cellular experiments, as described below.

Due to the cancer cell-targeting properties and the overall negatively charged nature of these obtained supramolecular nanoparticles, DOX, an anticancer drug that is widely used in tumor therapy, was chosen as a model drug to explore the photodynamic and chemotherapeutic performance of ternary assembly at the cellular level. The apparent binding affinity of DOX with HACD is known up to 10^4 M^{-1} .^{35,36} Therefore, through the UV–vis absorption standard curve of DOX at different concentrations, the encapsulation and loading efficiencies were calculated as 55.1 and 18.0%, respectively (Figure S13, Supporting Information). In addition, the presence of DOX did not change the morphology of the nanoparticulate assembly (Figure S10e, Supporting Information).

Cytotoxicity and Cell Imaging. Cytotoxicity experiments were conducted using the A549 human lung adenocarcinoma cells with abundant CD44 receptors on the cell surface and the 293T human embryonic kidney cells devoid of HA receptors as a control. Initially, the luminescence and distribution within cells were investigated by using confocal laser scanning microscopy (CLSM). The CLSM images in Figure 5 reveal that all the TPP-PY-involved groups were preferentially distributed in the mitochondria of A549 cells, and the TPP-PY/CB[8]@HACD assembly gave the highest Pearson correlation coefficient ($\rho \approx 0.6$, Figure S14, Supporting Information). This preferential accumulation is probably due to the more hyperpolarized membrane potentials at the mitochondria of cancer cells.^{37,38} Notably, when treated with the TPP-PY/CB[8]@HACD nanoparticles, the strongest red fluorescence was exclusively observed in A549 cells. As expected, lacking in the major surface hyaluronan receptors

(CD44), no obvious fluorescence was found in 293T cells under the same condition.

The ROS generation in the cells was assessed using 2,7-dichlorofluorescein diacetate (DCFH-DA) as a probe, where stronger green fluorescence positively correlates with higher ROS production. The data showed that among all the examined groups, the TPP-PY/CB[8]@HACD assembly exhibited the best ROS-generation ability in the cancer cells (Figure 6a). Moreover, the cell viability was explored before and after light irradiation by using the CCK-8 assay kit. The results indicated that TPP-PY only made minimal impact on the survival rates of two types of cells in the dark (Figure 6b,c). Meanwhile, the drug-loaded assembly always gave relatively lower cell viability even without light irradiation because of the DOX-induced cytotoxicity. However, after light irradiation, the viability of A549 cells was significantly decreased, while that of 293T cells was less pronounced. Apparently, these differences contributed to the HA-based cell targeting ability toward cancer cells, and the photodynamic effect became the dominant role for the enhanced cytotoxicity.

Taking the effective concentration of $1 \mu\text{M}$ as an example, the cell survival rate of two cell lines stayed at nearly 100% in the cases of free TPP-PY and the TPP-PY/CB[8] complex before light irradiation. In addition, this value was decreased to *ca.* 80% after loading DOX, and no significant difference was observed in these two cell lines at this stage. These results indicate the side effect of DOX on two cell lines. In contrast, as for the TPP-PY/CB[8]@HACD assembly, the viability of A549 cells sharply declined to only 22% after light irradiation at 650 nm, whereas more than 72% 293T cells remained alive under the same condition. In our case, both chemotherapeutic and photodynamic outcomes could be achieved in A549 cells at the concentrations of TPP-PY below $1 \mu\text{M}$. However, due to the rather low viability of only *ca.* 10% upon light irradiation, equivalent killing efficiency was found at $2 \mu\text{M}$ of TPP-PY in all four groups.

CONCLUSIONS

In summary, a supramolecular nanoassembly was successfully constructed by using the two-step host–guest complexation between CB[8] and tetracationic TPP-PY as a photosensitizer, as well as between HACD and DOX as a chemotherapeutic drug. The synthesized TPP-PY possesses good biocompatibility and a ROS generation efficiency. More remarkably, the fluorescence emission intensity of TPP-PY can be enhanced by the CB-confinement effect to weaken the intermolecular π – π stacking interaction. Moreover, ternary particulate assembly can be readily formed in the presence of HACD and DOX and can be efficiently loaded. Therefore, benefiting from the photosensitizing ability of the TPP-PY core and the cell-targeting ability of the HACD shell, the obtained TPP-PY/CB[8]@HACD nanoparticles can differentiate between cancer and normal cells and eventually induce the significant cytotoxicity in A549 cells after light irradiation. To be envisioned, the macrocycle-confined supramolecular nanoplat-form with synergistic drug delivery and photodynamic functions may enrich and expand the research of supramolecular nanomedicines for precision disease theragnosis.

ASSOCIATED CONTENT

Supporting Information

The Supporting Information is available free of charge at <https://pubs.acs.org/doi/10.1021/acsapm.4c00571>.

Synthesis and compound characterization, spectroscopic titration and calculation on binding constants and singlet oxygen yields, as well as drug loading and cell imaging results (PDF)

AUTHOR INFORMATION

Corresponding Authors

Ying-Ming Zhang – College of Chemistry, State Key Laboratory of Elemento-Organic Chemistry, Nankai University, Tianjin 300071, P. R. China; Email: ymzhang@nankai.edu.cn

Yu Liu – College of Chemistry, State Key Laboratory of Elemento-Organic Chemistry, Nankai University, Tianjin 300071, P. R. China; orcid.org/0000-0001-8723-1896; Email: yuliu@nankai.edu.cn

Authors

Xing Yuan – College of Chemistry, State Key Laboratory of Elemento-Organic Chemistry, Nankai University, Tianjin 300071, P. R. China

De-Fang Xu – Department of Anesthesiology, Tianjin Fourth Central Hospital, Tianjin 300140, P. R. China

Yahui Song – College of Chemistry, State Key Laboratory of Elemento-Organic Chemistry, Nankai University, Tianjin 300071, P. R. China

Complete contact information is available at:
<https://pubs.acs.org/10.1021/acsapm.4c00571>

Notes

The authors declare no competing financial interest.

ACKNOWLEDGMENTS

This work was financially supported by the Natural Science Foundation of Tianjin (21JCZDJC00310), the National Natural Science Foundation of China (grants 22171148, 22371148, and 22131008), and the Fundamental Research Funds for the Central Universities (Nankai University).

REFERENCES

- (1) Roy, I.; Garcıa, A.; Beldjoudi, Y.; Young, R. M.; Pe, D. J.; Nguyen, M. T.; Das, P. J.; Wasielewski, M. R.; Stoddart, J. F. Host-Guest Complexation-Mediated Supramolecular Photon Upconversion. *J. Am. Chem. Soc.* **2020**, *142*, 16600–16609.
- (2) Zhou, J.; Rao, L.; Yu, G.; Cook, T. R.; Chen, X.; Huang, F. Supramolecular Cancer Nanotheranostics. *Chem. Soc. Rev.* **2021**, *50*, 2839–2891.
- (3) Sun, C.; Wang, Z.; Yue, L.; Huang, Q.; Cheng, Q.; Wang, R. Supramolecular Induction of Mitochondrial Aggregation and Fusion. *J. Am. Chem. Soc.* **2020**, *142* (39), 16523–16527.
- (4) Huang, F.; Liu, J.; Li, M.; Liu, Y. Nanoconstruction on Living Cell Surfaces with Cucurbit[7]uril-Based Supramolecular Polymer Chemistry: Toward Cell-Based Delivery of Bio-Orthogonal Catalytic Systems. *J. Am. Chem. Soc.* **2023**, *145* (49), 26983–26992.
- (5) Sun, G.; Zuo, M.; Xu, Z.; Wang, K.; Wang, L.; Hu, X.-Y. Orthogonal Design of Supramolecular Prodrug Vesicles via Water-Soluble Pillar[5]arene and Betulinic Acid Derivative for Dual Chemotherapy. *ACS Appl. Bio Mater.* **2022**, *5*, 3320–3328.
- (6) Hao, M.; Sun, G.; Zuo, M.; Xu, Z.; Chen, Y.; Hu, X.-Y.; Wang, L. A Supramolecular Artificial Light-Harvesting System with Two-Step Sequential Energy Transfer for Photochemical Catalysis. *Angew. Chem., Int. Ed.* **2020**, *59*, 10095–10100.
- (7) Zhou, J.; Yu, G.; Yang, J.; Shi, B.; Ye, B.; Wang, M.; Huang, F.; Stang, P. J. Polymeric Nanoparticles Integrated from Discrete Organoplatinum (II) Metallacycle by Stepwise Post-assembly

Polymerization for Synergistic Cancer Therapy. *Chem. Mater.* **2020**, *32* (11), 4564–4573.

(8) Yang, J.; Dai, D.; Lou, X.; Ma, L.; Wang, B.; Yang, Y.-W. Supramolecular Nanomaterials Based on Hollow Mesoporous Drug Carriers and Macrocyclic-Capped CuS Nanogates for Synergistic Chemo-Photothermal Therapy. *Theranostics* **2020**, *10*, 615–629.

(9) Ma, Y.-L.; Yan, S.; Xu, X.-J.; Cao, H.; Wang, R. Synthetic Host-Guest Pairs as Novel Bioorthogonal Tools for Pre-Targeting. *Chin. Chem. Lett.* **2024**, *35*, 108645.

(10) Wu, X.; Gao, L.; Hu, X.-Y.; Wang, L. Supramolecular Drug Delivery Systems Based on Water-Soluble Pillar[n]arenes. *Chem. Rec.* **2016**, *16*, 1216–1227.

(11) Tian, X.; Zuo, M.; Niu, P.; Velmurugan, K.; Wang, K.; Zhao, Y.; Wang, L.; Hu, X.-Y. Orthogonal Design of a Water-Soluble meso-Tetraphenylethene-Functionalized Pillar[5]arene with Aggregation-Induced Emission Property and Its Therapeutic Application. *ACS Appl. Mater. Interfaces* **2021**, *13*, 37466–37474.

(12) Dai, X.; Huo, M.; Zhang, B.; Liu, Z.; Liu, Y. Folic Acid-Modified Cyclodextrin Multivalent Supramolecular Assembly for Photodynamic Therapy. *Biomacromolecules* **2022**, *23*, 3549–3559.

(13) Zhang, Y.-M.; Liu, Y.-H.; Liu, Y. Cyclodextrin-Based Multi-stimuli-Responsive Supramolecular Assemblies and Their Biological Functions. *Adv. Mater.* **2020**, *32*, 1806158.

(14) Mavridis, I. M.; Yannakopoulou, K. Porphyrinoid-Cyclodextrin Assemblies in Biomedical Research: An Update. *J. Med. Chem.* **2020**, *63*, 3391–3424.

(15) Yue, L.; Yang, K.; Lou, X.-Y.; Yang, Y.-W.; Wang, R. Versatile Roles of Macrocycles in Organic-Inorganic Hybrid Materials for Biomedical Applications. *Matter* **2020**, *3*, 1557–1588.

(16) Lim, W. Q.; Phua, S. Z. F.; Chen, H.; Zhao, Y. An Oxaliplatin(IV) Prodrug-Based Supramolecular Self-Delivery Nanocarrier for Targeted Colorectal Cancer Treatment. *Chem. Commun.* **2018**, *54*, 12762–12765.

(17) Zhang, Q.; Liu, F.; Nguyen, K. T.; Ma, X.; Wang, X.; Xing, B.; Zhao, Y. Multifunctional Mesoporous Silica Nanoparticles for Cancer-Targeted and Controlled Drug Delivery. *Adv. Funct. Mater.* **2012**, *22*, 5144–5156.

(18) Liu, Y.-H.; Zhang, Y.-M.; Yu, H.-J.; Liu, Y. Cucurbituril-Based Biomacromolecular Assemblies. *Angew. Chem., Int. Ed.* **2021**, *60*, 3870–3880.

(19) Wang, Z.; Sun, C.; Yang, K.; Chen, X.; Wang, R. Cucurbituril-Based Supramolecular Polymers for Biomedical Applications. *Angew. Chem., Int. Ed.* **2022**, *61*, No. e202206763.

(20) Yin, H.; Wang, R. Applications of Cucurbit[n]urils ($n = 7$ or 8) in Pharmaceutical Sciences and Complexation of Biomolecules. *Isr. J. Chem.* **2018**, *58*, 188–198.

(21) Gao, L.; Wang, H.; Zheng, B.; Huang, F. Combating Antibiotic Resistance: Current Strategies for the Discovery of Novel Antibacterial Materials Based on Macrocyclic Supramolecular Chemistry. *Giant* **2021**, *7*, 100066.

(22) Xu, D.-A.; Zhou, Q.-Y.; Dai, X.; Ma, X.-K.; Zhang, Y.-M.; Xu, X.; Liu, Y. Cucurbit[8]uril-Mediated Phosphorescent Supramolecular Foldamer for Antibiotics Sensing in Water and Cells. *Chin. Chem. Lett.* **2022**, *33*, 851–854.

(23) Dai, X.-Y.; Huo, M.; Liu, Y. Phosphorescence Resonance Energy Transfer from Purely Organic Supramolecular Assembly. *Nat. Rev. Chem.* **2023**, *7*, 854–874.

(24) Dai, X.-Y.; Huo, M.; Dong, X.; Hu, Y.-Y.; Liu, Y. Noncovalent Polymerization-Activated Ultrastrong Near-Infrared Room-Temperature Phosphorescence Energy Transfer Assembly in Aqueous Solution. *Adv. Mater.* **2022**, *34*, 2203534.

(25) Hu, H.; Wang, H.; Yang, Y.; Xu, J.-F.; Zhang, X. A Bacteria-Responsive Porphyrin for Adaptable Photodynamic/Photothermal Therapy. *Angew. Chem., Int. Ed.* **2022**, *61*, No. e202200799.

(26) Mao, Q.; Kitagishi, H. Inclusion Complex Formation with Tetra-PEGylated Tetraphenylporphyrin and Face-to-Face Cyclodextrin Dimer through Unprecedented Molecular Threading. *Chem.—Eur. J.* **2023**, *29*, No. e202300408.

(27) Yang, Y.; Zhang, Y.-M.; Chen, Y.; Chen, J.-T.; Liu, Y. Targeted Polysaccharide Nanoparticle for Adamplatin Prodrug Delivery. *J. Med. Chem.* **2013**, *56*, 9725–9736.

(28) Li, Y.; Qin, C.; Li, Q.; Wang, P.; Miao, X.; Jin, H.; Ao, W.; Cao, L. Supramolecular Organic Frameworks with Controllable Shape and Aggregation-Induced Emission for Tunable Luminescent Materials through Aqueous Host-Guest Complexation. *Adv. Optical Mater.* **2020**, *8*, 1902154.

(29) Chen, X.; Bisoyi, H. K.; Chen, X.-F.; Chen, X.-M.; Zhang, S.; Tang, Y.; Zhu, G.; Yang, H.; Li, Q. Hierarchical Self-Assembly of an Excitation-Wavelength-Dependent Emissive Fluorophore and Cucurbiturils for Secondary Encryption. *Matter* **2022**, *5*, 3883–3900.

(30) Li, Z.-Q.; Zhang, Y.-M.; Chen, Y.; Liu, Y. A Supramolecular Tubular Nanoreactor. *Chem.—Eur. J.* **2014**, *20*, 8566–8570.

(31) Liu, Z.; Lin, W.; Liu, Y. Macrocyclic Supramolecular Assemblies Based on Hyaluronic Acid and Their Biological Applications. *Acc. Chem. Res.* **2022**, *55*, 3417–3429.

(32) Tang, M.; Song, Y.; Lu, Y.-L.; Zhang, Y.-M.; Yu, Z.; Xu, X.; Liu, Y. Cyclodextrin-Activated Porphyrin Photosensitization for Boosting Self-Cleavable Drug Release. *J. Med. Chem.* **2022**, *65*, 6764–6774.

(33) Tang, M.; Liu, Y.-H.; Liu, H.; Mao, Q.; Yu, Q.; Kitagishi, H.; Zhang, Y.-M.; Xiao, L.; Liu, Y. Supramolecular Dual Polypeptides Induced Tubulin Aggregation for Synergistic Cancer Theranostics. *J. Med. Chem.* **2022**, *65*, 13473–13481.

(34) Niu, J.; Liu, Y.-H.; Xu, W.; Xu, W.-W.; Song, Y.-H.; Yu, J.; Zhang, Y.-M.; Liu, Y. Morpholine-modified permethyl β -cyclodextrin supramolecular nanoparticles for precise dual-targeted imaging. *Chem. Commun.* **2023**, *59*, 4680–4683.

(35) Bognanni, N.; Viale, M.; La Piana, L.; Strano, S.; Gangemi, R.; Lombardo, C.; Cambria, M. T.; Vecchio, G. Hyaluronan-Cyclodextrin Conjugates as Doxorubicin Delivery Systems. *Pharmaceutics* **2023**, *15*, 374–384.

(36) Fülöp, Z.; Kurkov, S. V.; Nielsen, T. T.; Larsen, K. L.; Loftsson, T. Self-Assembly of Cyclodextrins: Formation of Cyclodextrin Polymer Based Nanoparticles. *J. Drug Delivery Sci. Technol.* **2012**, *22*, 215–221.

(37) Kolb, D.; Kolishetti, N.; Surnar, B.; Sarkar, S.; Guin, S.; Shah, A. S.; Dhar, S. Metabolic Modulation of the Tumor Microenvironment Leads to Multiple Checkpoint Inhibition and Immune Cell Infiltration. *ACS Nano* **2020**, *14*, 11055–11066.

(38) Wang, H.; Song, Y.; Wang, W.; Chen, N.; Hu, B.; Liu, X.; Zhang, Z.; Yu, Z. Organelle-Mediated Dissipative Self-Assembly of Peptides in Living Cells. *J. Am. Chem. Soc.* **2024**, *146*, 330–341.

NOTE ADDED AFTER ASAP PUBLICATION

This paper was published ASAP on March 29, 2024, with an incorrect version of Figure 4. The corrected version was reposted on April 2, 2024.